Simultaneous radio and optical observations of auroral structures: Implications for AKR beaming

J. D. Menietti,[1] R. L. Mutel,[1] I. W. Christopher,[1] K. A. Hutchinson,[1] and J. B. Sigwarth[2,3]

Received 16 September 2011; revised 9 November 2011; accepted 16 November 2011; published 17 December 2011.

[1] Polar spacecraft observations of auroral kilometric radiation (AKR) spectra, combined with simultaneous optical images of the auroral oval at the source foot points, show a strong correlation with discrete auroral features. We discuss several examples of distinctive "V"-shaped profiles in time-frequency AKR spectra for which the time of nadir passage (bottom of V) coincides with the spacecraft crossing field lines connected to discrete auroral arcs. These results support models of AKR emission originating in density cavities with radiation initially confined to a "tangent plane" but strongly refracted upward in a frequency-dependent manner. The inferred spatial distributions of AKR sources are closely coincident with field lines connecting discrete auroral arcs, indicating that discrete arcs are highly correlated with robust AKR emission on the same field lines, as first suggested by Gurnett (1974) several decades ago.

Citation: Menietti, J. D., R. L. Mutel, I. W. Christopher, K. A. Hutchinson, and J. B. Sigwarth (2011), Simultaneous radio and optical observations of auroral structures: Implications for AKR beaming, *J. Geophys. Res.*, *116*, A12219, doi:10.1029/2011JA017168.

1. Introduction

[2] *Gurnett*'s [1974] landmark paper describing the properties of auroral kilometric radiation (AKR) included a discussion of the association between AKR occurrence and the presence of discrete auroral arcs. Although the paper established a clear temporal correlation, it was not obvious whether there was a direct connection: Were AKR and auroral arcs modulated by the same physical trigger, or were auroral brightenings and AKR emission simply two independent indicators of enhanced geomagnetic activity?

[3] A few years later, satellite measurements above the auroral zone [e.g., *Benson and Calvert*, 1979] found downward-going electron beams in density-depleted cavities containing AKR sources, which strengthened the case for a physical association between the AKR emission and auroral arcs. In a well-cited study, *Huff et al.* [1988] showed the first examples of simultaneous AKR emission and aurora activity along the same field line. Using the PWI radio instrument and the visible-ultraviolet imager on the DE-1 spacecraft, they showed several examples of intense coeval AKR emission on field lines connected to bright auroral features. Subsequently, simultaneous optical-radio observations with the Viking spacecraft [*de Feraudy et al.*, 1987; *Bahnsen et al.*, 1987, 1989; *Pedersen et al.*, 1992] provided additional examples of auroral features well-correlated with AKR emission located on the same magnetic field lines. These observations, as well as more recent AKR source region measurements by the FAST mission [e.g., *Delory et al.*, 1998; *Ergun et al.*, 1998], established the now well-accepted view that both AKR and auroral emission are excited by downward beams of mildly relativistic electrons residing in density-depleted cavities.

[4] The role of the auroral cavities in channeling AKR radiation was first studied by *Bahnsen et al.* [1987] and *de Feraudy et al.* [1987]. Previous AKR beaming studies had found large-angled, filled emission cones [*Green et al.*, 1977; *Green and Gallagher*, 1985], as well as hollow cone patterns [*Calvert*, 1981, 1987]. However, *de Feraudy et al.* [1987] suggested that the radiation pattern would be constrained by the cavity walls, leading to an asymmetric pattern aligned along the cavity longitudinal axis. *Bahnsen et al.* [1987] found that the characteristic bell-shaped broadband morphology seen in AKR dynamical spectra could be explained by frequency-dependent upward refraction as the satellite passes over an active field line. *de Feraudy and Schreiber* [1995] performed ray-tracing analysis to predict that the radiation pattern was oval-shaped with the major axis oriented along the auroral cavity, a consequence of the auroral cavity walls confining the radiation in the latitudinal direction. Additional ray-tracing studies of AKR spectra obtained from the Interball-2 satellite [*Schreiber et al.*, 2002; *Schreiber*, 2005] substantiated these ideas.

[5] Since the beaming pattern is highly directional, a single spacecraft at a given location will only detect AKR emission from a relatively small frequency-dependent footprint in the auroral zone. *Mutel et al.* [2008] used the WBD receivers from four spacecraft on the Cluster constellation [*Gurnett et al.*, 2001] to triangulate AKR source locations that were mutually visible at all spacecraft locations. They analyzed

[1]Department of Physics and Astronomy, University of Iowa, Iowa City, Iowa, USA.
[2]Goddard Space Flight Center, Greenbelt, Maryland, USA.
[3]Deceased 13 December 2010.

Copyright 2011 by the American Geophysical Union.
0148-0227/11/2011JA017168

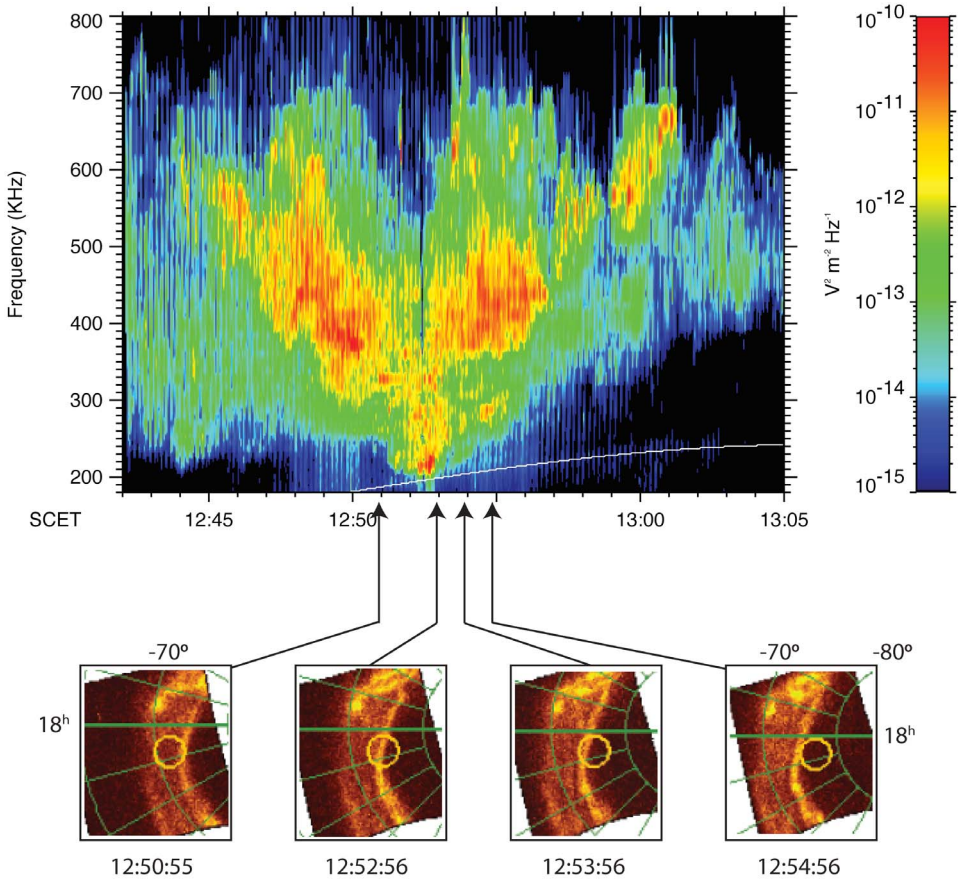

Figure 1. (top) Polar PWI time-frequency spectrum of AKR emission on 22 June 1997 from 12:40 — 13:05 SCET showing a characteristic "V" spectral pattern. The spacecraft was at an altitude ~6,400 km in the Southern hemisphere near magnetic local time 19 hr and magnetic latitude -70°. (bottom) Polar VIS images taken between 12:50:55 SCET and 12:54:50 SCET. The yellow circle indicates the position of spacecraft projected along a constant magnetic field line to the ionosphere. Note the time coincidence between crossing the bottom of the "V" feature (12:52:30) and crossing field lines connected to the bright discrete auroral arc. The white line indicates the local electron cyclotron frequency at the spacecraft.

several thousand events to determine a statistical angular beaming pattern, which was highly confined latitudinally (typically ±15° from the magnetic field tangent direction), but much wider longitudinally, i.e., along the cavity. In this "tangent plane" model, the emission is refracted upward in a beam pattern that propagates primarily in the low-density plane of the field-aligned current sheet, hence along the auroral arc, in qualitative agreement with previous observational studies cited above, and with the analytic model of *Louarn and Le Quéau* [1996] and PIC plasma simulations of radiation in low-density cavities [*Pritchett et al.*, 2002].

[6] In this paper we provide new observational evidence for both the association of intense AKR emission with discrete auroral arcs and for the tangent plane beaming model. We analyze AKR spectra obtained by Plasma Wave Instrument (PWI) on board the Polar spacecraft, in conjunction with simultaneous high spatial-resolution auroral images obtained by the Visible Imaging System (VIS), also on board Polar. We analyze three events for which there are distinct auroral arcs features in the VIS images, and for which there is intense AKR emission. The dynamic spectra show a distinctive "V" shaped AKR morphology centered on times when the spacecraft magnetic footprint intersects the magnetic field line connected with discrete auroral arc structures. We model the source region as a thin sheet of elementary "sourcelets" generating AKR emission at the local electron cyclotron frequency. We use ray-tracing to determine the predicted beaming pattern of the AKR emission as a function of frequency, and compare with observed spectra.

2. An Illustrative Example: Event of 22 June 1997

[7] We first illustrate the AKR — auroral arc connection with an sample event showing the close association between a discrete auroral arc and a coeval AKR spectral signature. In the following section, we describe a simple emission geometry and beaming model which fits the AKR spectrum and predicts the location of discrete auroral arc at the base of the emission sheet. We then apply this model to three events, including an interesting "double arc" case.

[8] Figure 1 (top) shows a frequency-time spectrogram of PWS magnetic antenna data for June 22, 1997 from 12:40 to 13:05 SCET. The intense AKR emission has a characteristic

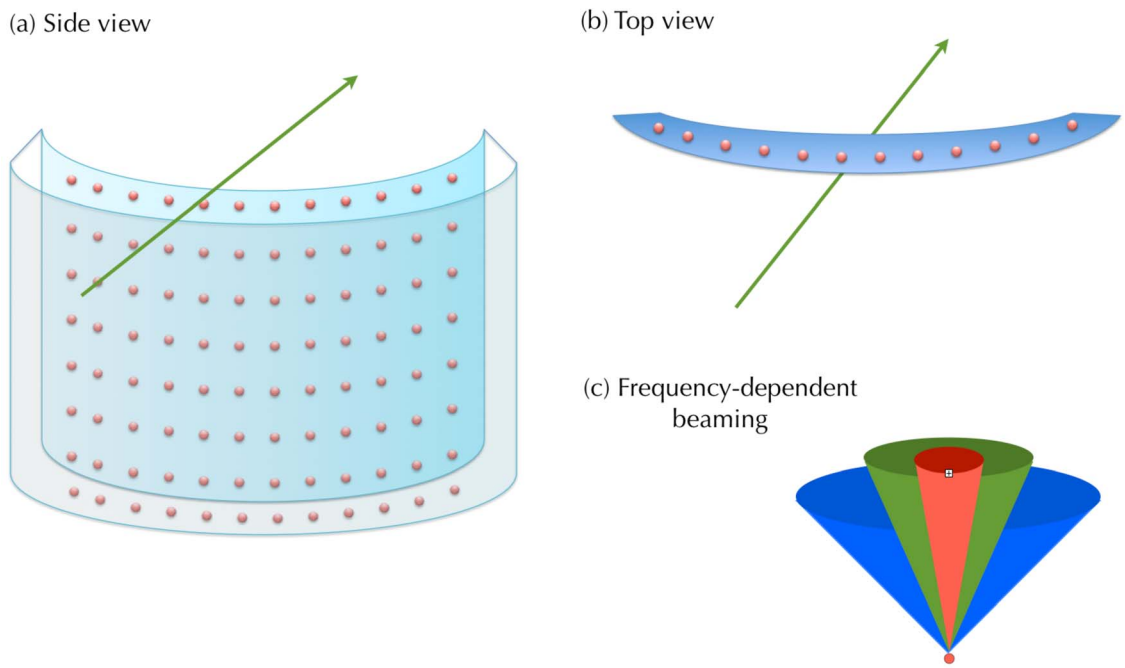

Figure 2. Geometry of the AKR source tangent plane model. The AKR source region is confined to a thin auroral sheet ("tangent plane") populated by many uniformly spaced elementary AKR sources (red dots), each radiating at the local electron cyclotron frequency. There are 30 sources per row spanning 3 hr MLT, and 30 rows spanning 190 KHz — 600 KHz depth. (a and b) Side and top views of the AKR region respectively, along with a representative spacecraft trajectory (green line). (c) Illustration of the asymmetric frequency-dependent angular beaming, with orientation of the beaming ellipses along the tangent plane. The red, green, and blue cones illustrate angular patterns of increasing frequency. The exact beaming parameters were best-fit for each event (see text for details).

V-shaped pattern, similar to previously published "dish-shaped" AKR spectra [e.g., *Bahnsen et al.*, 1987; *Hanasz et al.*, 2001]. The white line indicates the local electron cyclotron frequency (f_{ce}) at the spacecraft. The minimum frequency of the emission is at or slightly below the value of f_{ce} near 12:52:30. The emission at f_{ce} is very intense at this time, since the spacecraft is located very near or possibly within the source region.

[9] Figure 1 (bottom) shows a series of auroral images obtained by the VIS instrument. The time of each image is indicated by the black arrows connecting each VIS image to the time axis. The circle on each figure indicates the footprint of the magnetic field line that passes through the spacecraft, based on mapping using the *Tsyganenko* [1989] magnetic field model. The spacecraft field line footprint traverses a bright discrete arc during the event. When the footprint is closest to the discrete arc near 12:53:00, the spacecraft is within the AKR source region and the minimum frequency of AKR is observed as seen in Figure 1. This is compelling empirical evidence that the discrete arc is located along the same active field line and is excited by the same electron beam that is driving the cyclotron maser instability (CMI) responsible for the AKR emission.

3. Tangent Plane AKR Beaming Model

[10] We model the AKR source region as the aggregate emission from a large number of identical, uniformly spaced elementary sources ("sourcelets") residing in a thin sheetlike structure, as shown in Figure 2. There are 30 sources per row spanning the MLT range of the model arc and 30 rows spaced at altitudes corresponding to a uniform span of electron cyclotron frequency, from 190 — 600 KHz. The sheet is confined latitudinally along magnetic field lines passing through a fixed magnetic latitude λ_c. The central MLT and λ_c were adjusted to provide a best-fit to the observed spectrum as described below. For two of the events (16 May 1997, 22 June 1997) we modeled the emission with a single arc, while for 30 July 1997 we summed the contributions from two arcs.

[11] We use a magnetospheric density model based on *Denton et al.* [2004], but with two modifications. First, since the Denton et al. model only extends to L-shell $L \sim 8$, we added a simple quadratic power law density profile at high latitude,

$$n_e(r) = n_{e0}\left(\frac{r}{r_o}\right)^{-2}$$

where $n_{e0} = 100\ \mathrm{cm}^{-3}$ and r_0 is the Earth radius. Second, we add a density-depleted cavity on the active field line corresponding to the L-shell of the discrete arc in the VIS image. The cavity is aligned along the active L-shell and has a density profile in latitude given by

$$n_c(r, L) = n_{c0} + n_d(r, L) \cdot \tanh\left(\frac{|\mathrm{L} - \mathrm{L_c}|}{\sigma_\mathrm{c}}\right)$$

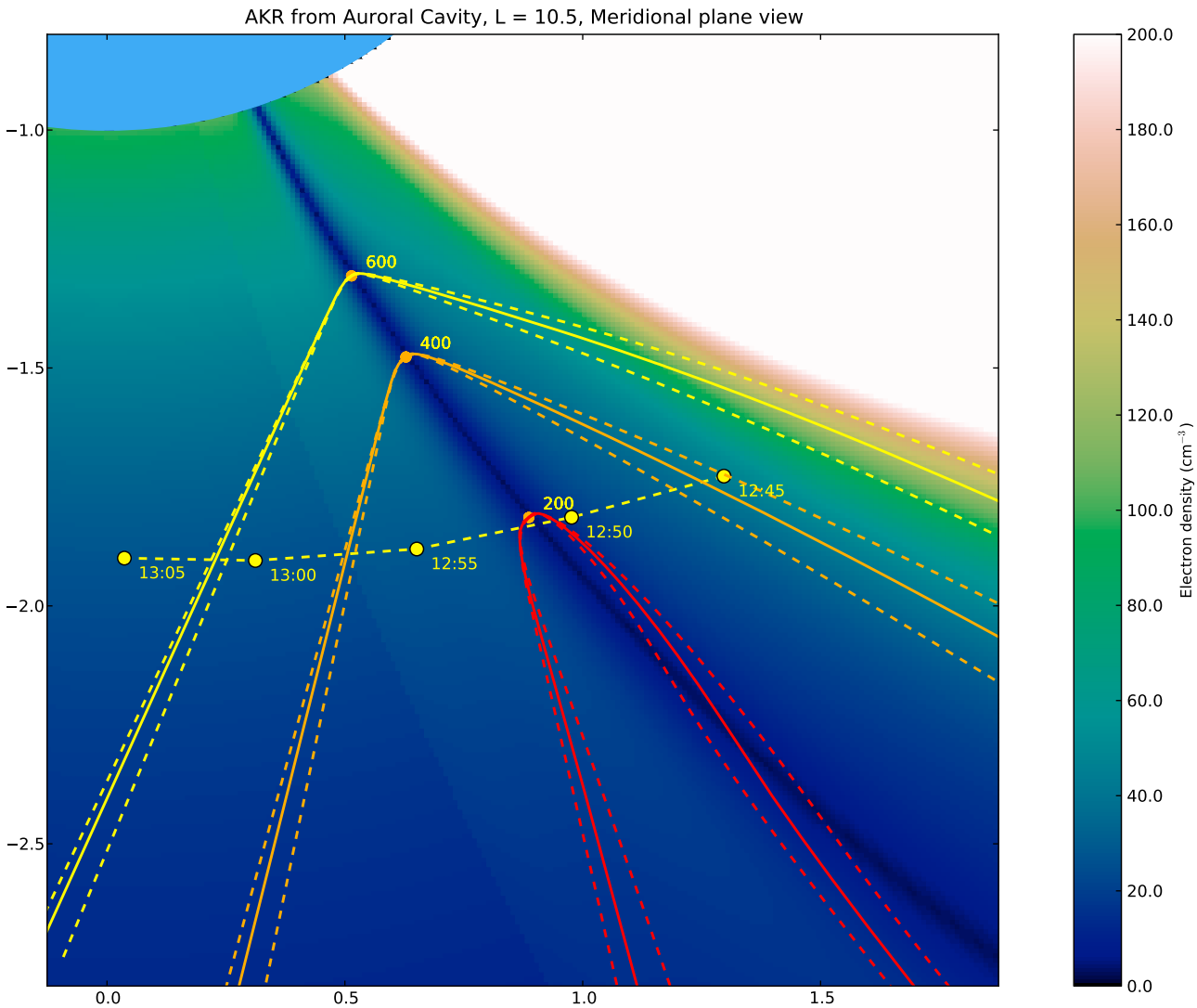

Figure 3. Calculated AKR raypaths and auroral zone geometry of the 22 June 1997 event. Rays originate in an auroral cavity (n_e = cm^{-3}) at L-shell 10.5 ($\lambda_m = -72°$) at altitudes corresponding to electron cyclotron frequencies 200 KHz (red lines), 400 KHz (orange lines), and 600 KHz (yellow lines). For each frequency, the solid lines are rays generated at 90° initial wave normal angle, while dotted lines are at 85° and 95°. The yellow dashed line labeled with time stamps shows the trajectory of the Polar spacecraft projected onto a meridian plane between 12:45 and 13:05 SCET, when the dynamic spectrum shown in Figure 1 was observed. Note the frequency-dependent upward-going refraction pattern and the frequency-time correspondence between the ray-tracing and the observed spectrum.

where n_{c0} is the density at the center of the cavity, $n_d(r,L)$ is the *Denton et al.* [2004] density profile, L_c is the center L-shell of the cavity, and σ_c is the characteristic cavity width. For all three cases presented in this paper, we used n_{c0} = 3 cm^{-3} and σ_c = 2. Changing these values by a modest amount (factor of 2 in each case) changed the detailed propagation paths, but did not significantly change the qualitative model fit.

[12] Each sourcelet has identical luminosity, but a beaming pattern which depends on frequency. The beaming pattern was determined by calculating X-mode raypaths using a numerical implementation of the Hamiltonian raypath equations [*Haselgrove*, 1963]. Sample raypaths for the 22 June 1997 event are shown in Figure 3. We show three sample sourcelet rays, at altitudes corresponding to cyclotron frequencies 200 KHz, 400 KHz, and 600 KHz. The solid lines show rays with initial wave-normal angles ±90°, while the dashed rays are at ±85°, and ±95°. Since the cyclotron maser instability (CMI) driven by a shell-type electron velocity distribution has the largest growth rate for X-mode emission near perpendicular wave-normal angle[*Treumann*, 2006; *Mutel et al.*, 2007], we only consider rays at perpendicular launch (initial wave-normal) angle, and do not consider raypaths at oblique angles.

[13] Figure 3 also shows the path of the Polar spacecraft on 22 June 1997 from 12:45 — 13:05 SCET. The spacecraft path makes an oblique angle with respect to the meridian plane; We show its projection onto the meridian plane containing the active field line. Comparing the observed time-frequency spectrum in Figure 1 with the time of interception

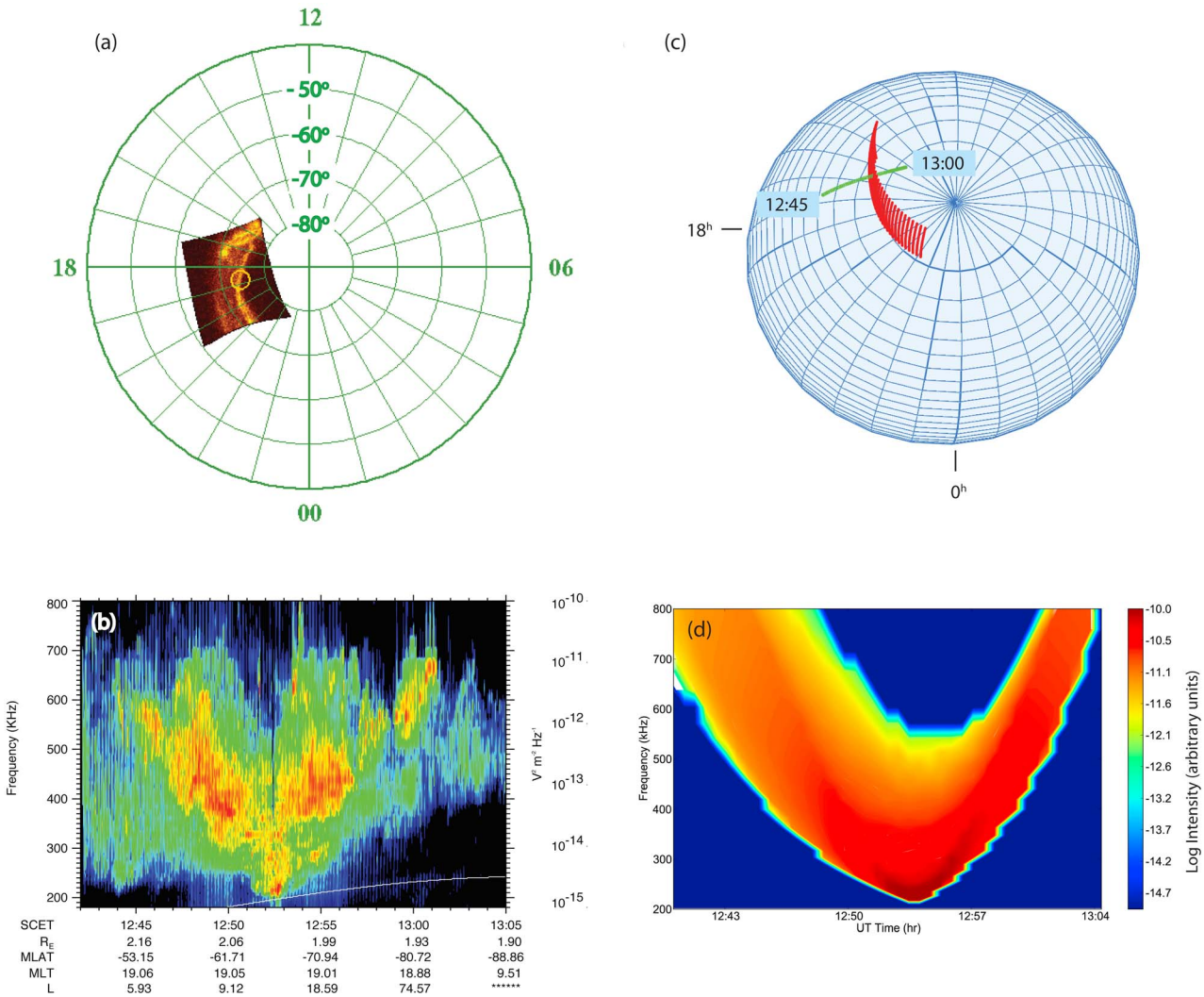

Figure 4. (a) Polar VIS auroral image taken on 22 June 1997 at 12:52:56 SCET projected onto CGM coordinate grid. Yellow circle indicates magnetic foot point of Polar spacecraft at 12:52:56 SCET at nadir of spectral "V." (b) Polar PWS dynamical spectrum between 12:40 and 13:05 SCET. (c) Three-dimensional perspective view of spacecraft trajectory and locations of AKR sources in tangent plane model producing the best-fit model spectrum. (d) Synthetic spectrum generated by tangent plane AKR model as shown in Figure 2.

of the raypaths, it is clear that the V shaped AKR spectra is a consequence of the frequency-dependent refraction of the rays.

[14] Since the ray tracing algorithm is currently 2-dimensional, we restricted the ray calculations to the meridian plane and did not calculate longitudinal raypaths. Rather, we used the results of *Mutel et al.* [2008], who found that the longitudinal beam width was much larger than the latitudinal width. We assumed that the longitudinal beam pattern was isotropic, at least over the limited range of longitudinal angles between the sourcelets and the spacecraft locations (not more than 50°).

[15] For all three events discussed below, we constructed model time-frequency spectra by summing the contributions from all 900 sourcelets at each spacecraft location using a r^{-2} intensity weighting function. We adjusted the central MLT and magnetic latitude of the AKR sourcelet sheet so that the model spectra most resembled the observed AKR spectrum. For some cases, several closely spaced MLT and magnetic latitude ranges were needed to reproduce the observed spectrum. We then mapped the locus of all AKR sourcelets that contributed to the model spectrum and traced their foot points to the base of the auroral zone. This provides a critical test for the AKR — discrete auroral arc hypothesis viz, comparing how closely the field lines associated with AKR emission corresponded to those threading the discrete auroral arcs seen in the VIS images.

4. Comparison With AKR Source Model

4.1. The 22 June 1997 Event

[16] Figure 4 shows the same VIS image (Figure 4a) and time-frequency spectrum (Figure 4b) for the 22 June 1997 event for reference. Figure 4c is a 3-dimensional perspective

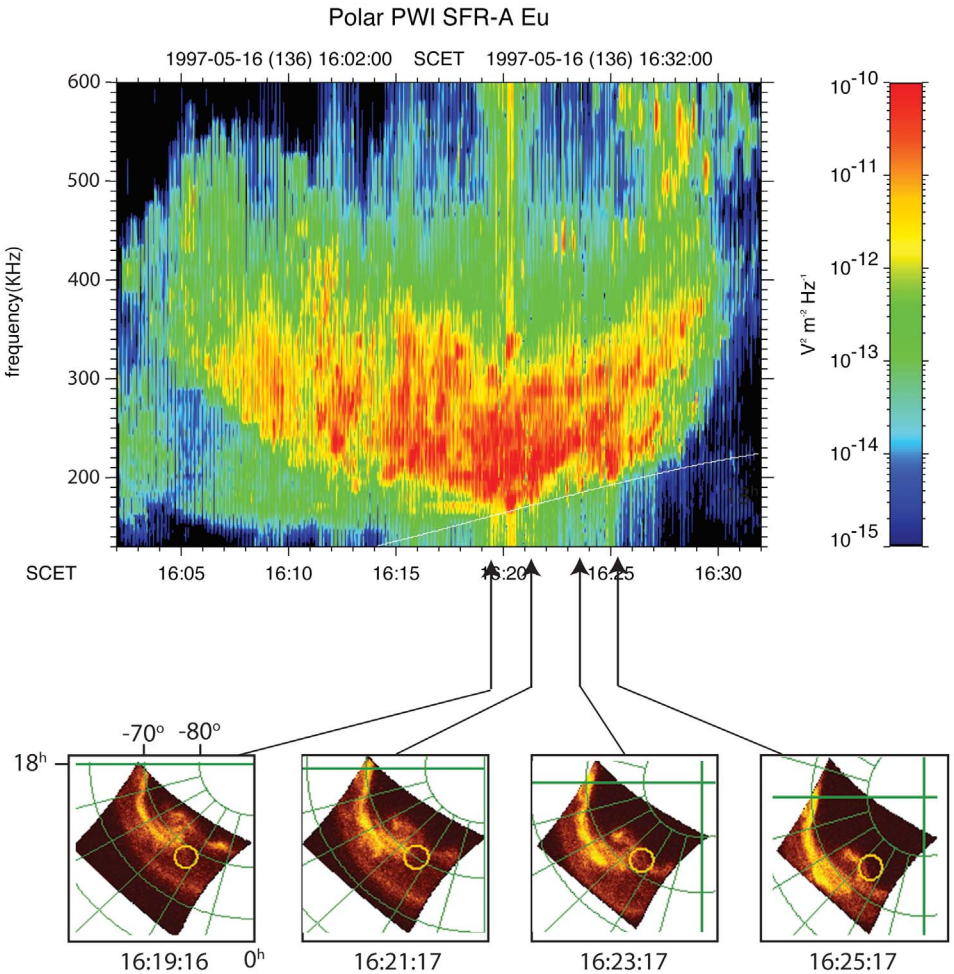

Figure 5. (top) Polar PWI time-frequency spectrum of AKR emission on 16 May 1997 from 16:02 — 16:32 SCET. The spectrum has a characteristic "V" spectral pattern with a source crossing ($f = f_{ce}$) near 16:20 SCET, but the spectral shape is flatter and significantly asymmetric compared with spectrum on 22 June 1997 (cf. Figure 1). There is also a second source crossing 16:25 SCET. (bottom) Polar VIS images taken between 16:19:19 SCET and 16:25:17 SCET. The yellow circle indicates the position of spacecraft projected along a constant magnetic field line to the ionosphere. The spacecraft trajectory - auroral arc angle is much smaller than the 22 June 1997 event, resulting in the shallower "bowl-like" spectral shape. The trajectory also crosses two auroral arc features (the second less distinct), consistent with the double source crossing (see text).

view of the AKR sourcelet sheet and the spacecraft trajectory. Figure 4d shows the model spectrum computed by summing the contributions from all AKR sourcelets in the sheet. The source locus footprint map is in excellent agreement with the discrete arc location, as is the model time-frequency spectrum with the observed spectrum. Note that the spacecraft trajectory crosses nearly perpendicular to the AKR emission region, so that the spectral "V" pattern is nearly identical on both sides of the nadir at 12:52:30.

4.2. The 16 May 1997 Event

[17] A second example of an AKR emission region transit is shown in Figure 5. Figure 5 (top) shows the PWI time-frequency spectrum of an intense "V"-shaped AKR burst with the sheet crossing ($f \sim f_{ce}$) just after 16:20 SCET, and a less intense second sheet crossing near 16:25 SCET. Figure 5 (bottom) shows VIS images taken at 120-sec intervals from 16:19:16 — 16:25:17 SCET, with the yellow circles indicating the foot points of the magnetic field line of the spacecraft at the time of each frame. The spectral shape is less V-shaped compared with the 22 June event, and is also somewhat asymmetric. Note that both source crossing times (i.e., where $f = f_{ce}$) closely match the transit times of discrete aurora arc features.

[18] Figure 6 shows the results of the tangent plane model fit in the same format as Figure 4. The more flattened bowl shape of the observed spectrum is also evident in the model spectrum, as is the asymmetry with respect to the spectral nadir at 16:20 SCET. Both effects result from the nearly tangential trajectory of the spacecraft with respect to the auroral arc. The time of source passage (nadir of "V" shape, and $f = f_{ce}$), 16:20 SCET, agrees very well with the spacecraft foot point transit of the large auroral arc evident on the VIS images. Also, the locus of footprint points matches the

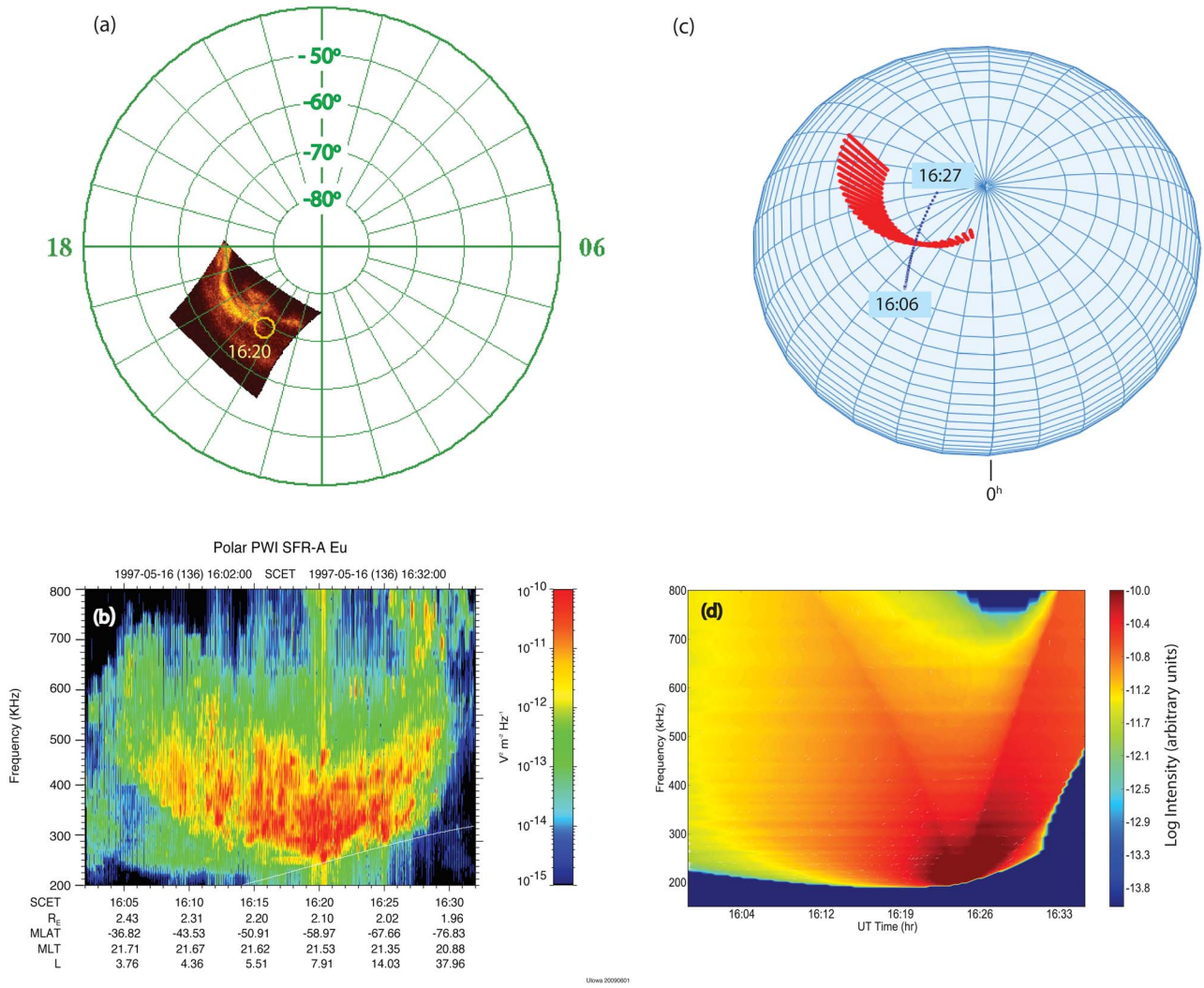

Figure 6. (a) Polar VIS auroral image taken on 16 May 1997 at 16:20:16 SCET projected onto CGM coordinate grid. Yellow circle indicates magnetic foot point of Polar spacecraft at 16:20:16 SCET at nadir of spectral "V." (b) Polar PWS dynamical spectrum between 16:00 and 16:32 SCET. (c) Three-dimensional perspective view of spacecraft trajectory and locations of AKR sources in tangent plane model producing the best-fit model spectrum. (d) Synthetic spectrum generated by tangent plane AKR model sourcelets as shown in Figure 6.

large discrete arc very well. Although we did not model the much smaller, less intense arc at magnetic latitude $\lambda_m \sim -75°$ and MLT~20 —23, it is clearly associated with the second AKR source crossing near 16:25 SCET, since the time of arc transit matches the AKR source passage time.

4.3. The 30 July 1997 Event

[19] The third event, observed on 30 July 1997, is shown in Figure 7. A VIS auroral image (Figure 7a) was taken at 03:15 SCET. It shows an extended bright auroral feature extending from magnetic latitude −65° to −75° and across the entire MLT range of the image, from 19 hr - 02 hr. Although the structure is very extended, there are two bright arcs that can be identified, in the range $-68° \leq \lambda_m \leq -70°$ and 19.5 < MLT < 23 (labeled Arc 1) and $\lambda_m \sim -74°$ and 0 < MLT < 2 (labeled Arc 2). We have also shown the foot points of the Polar spacecraft (labeled yellow dots) as it traversed the active region from 03:10 to 0325 SCET.

[20] The observed spectrum (Figure 7b) has two clearly identifiable dish-like features, centered near 03:08 SCET and 03:13 SCET. Motivated by the two discrete arc structures and the two-dish spectral signature, we constructed a model with two AKR sourcelet sheets. Each sheet was placed at the magnetic latitude and MLT range corresponding to the discrete arc in the VIS image. These are shown in Figure 7c, along with the trajectory of the Polar spacecraft from 03:00 — 3:30. The synthetic time-frequency spectrum using these source sheets is shown in Figure 7d. Once again, the agreement with the observed spectrum is quite good. The spacecraft trajectory crossed the first source sheet, so that the frequency at the nadir of the first dish-like feature ($f \sim$ 220 KHz) is approximately equal to the electron cyclotron frequency. However, the trajectory does not intercept the

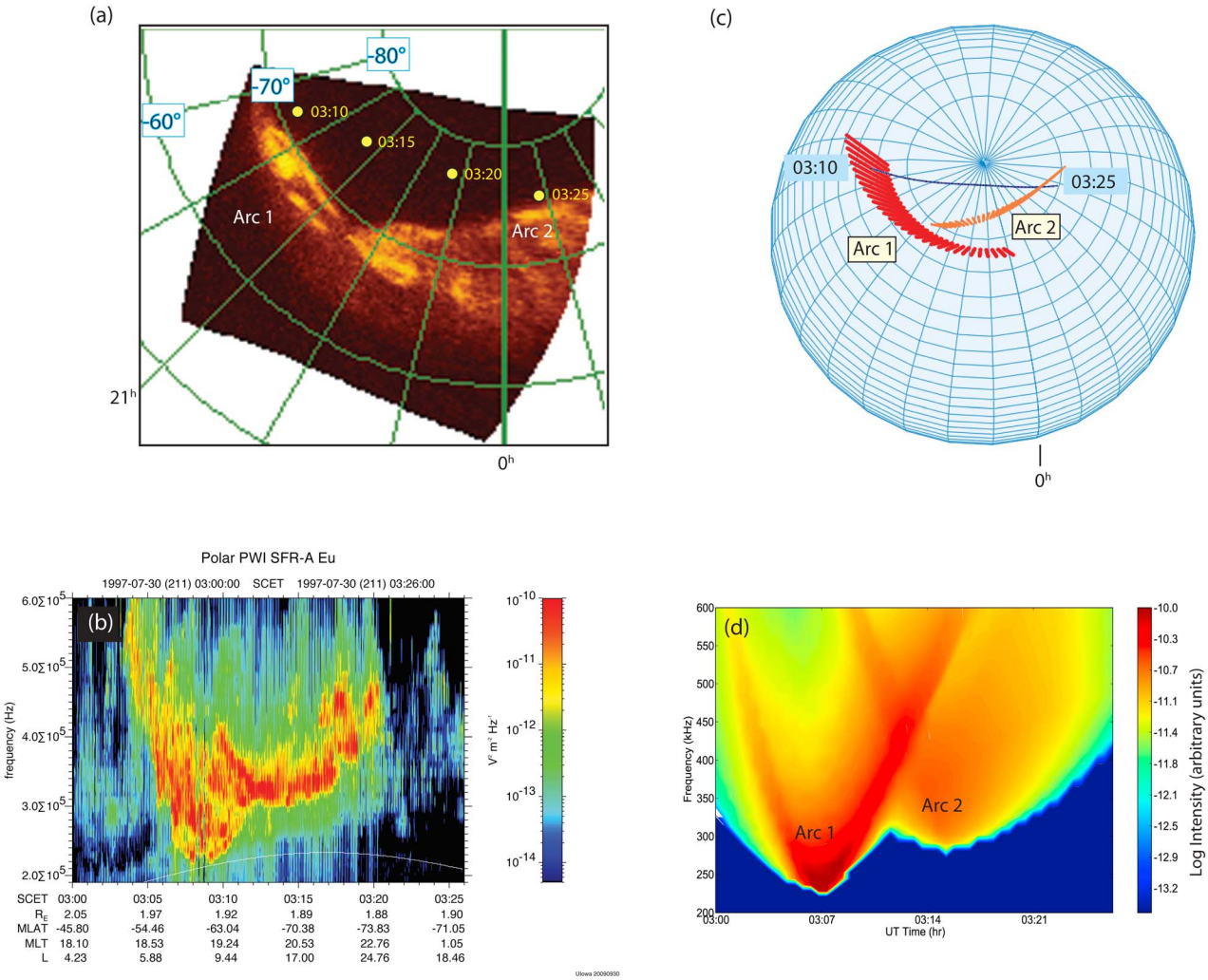

Figure 7. (a) Polar VIS auroral image taken on 30 July 1997 at 03:03:37 SCET projected onto CGM coordinate grid. Yellow dots indicate magnetic foot points of Polar spacecraft projected onto CGM coordinate grid at labeled times. (b) Polar PWS dynamical spectrum between 03:00 and 03:25 SCET. (c) Three-dimensional perspective view of Polar spacecraft trajectory over southern auroral region from 03:00 — 03:30 SCET showing AKR sourcelet sheets for arcs 1 and 2. (d) Synthetic spectrum generated by tangentplane AKR model sourcelets shown in Figure 7c and observed along Polar spacecraft trajectory.

second AKR source sheet (cf. Figure 7c), of the frequency minimum of the second spectral feature ($f \sim 330$ KHz), which is well above the local cyclotron frequency ($f_{ce} \sim 230$ KHz).

5. Summary and Conclusions

[21] We have presented three examples of Polar satellite passes through AKR source regions observed by the plasma wave instrument. In these cases, selected from a larger number of similar passes, we also present VIS auroral image data indicating that the spacecraft traversed a region associated with one or more discrete auroral arcs located along the same magnetic field lines as the AKR source region.

[22] In each case, we modeled the AKR source using a thin vertical sheet of identical elementary sources ("sourcelets") radiating at the local electron cyclotron frequency. The propagation paths of the sourcelet emissions were calculated by assuming that the AKR sources were located in a density-depleted cavity. We calculate x-mode raypaths using a numerical Hamiltonian ray approximation. The rays were launched at perpendicular propagation, but were strongly refracted upward in a frequency-dependent manner as they exited the cavity. By summing the distance-weighted contributions from all sourcelets at each spacecraft location, we constructed synthetic spectra and foot point locations of the sheet to compare with observations. In all three cases, we were able to closely match the observed spectral features. We also found that the foot points of the AKR source region sheet closely matched the location of bright aurora arcs seen in the VIS images.

[23] These results confirm that discrete arcs and source regions of intense AKR are often located on the same active field lines. They also substantiate models of AKR generation

and propagation in which the CMI instability generates radiation most intensely near perpendicular propagation, but the rays are strongly refracted by the region as they escape low-density cavities into regions of higher density plasma outside the current sheet. These model results also strongly support the AKR "tangent plane"beaming models based on Viking observations [*de Feraudy and Schreiber*, 1995; *Louarn and Le Quéau*, 1996], numerical PIC simulations of AKR radiation in cavities [*Pritchett et al.*, 2002], and by Cluster interferometry observations [*Mutel et al.*, 2008].

[24] **Acknowledgments.** We wish to thank J. Barnholdt and K. Kurth for clerical assistance. This work was supported by NSF award ATM-0407155 and by NASA grant NNX07AI24G with Goddard Space Flight Center. We thank R. Dvorsky for providing VIS images with explanation.

[25] Robert Lysak thanks Roman Schreiber and another reviewer for their assistance in evaluating this paper.

References

Bahnsen, A., M. Jespersen, E. Ungstrup, and I. B. Iversen (1987), Auroral hiss and kilometric radiation measured from the Viking satellite, *Geophys. Res. Lett.*, *14*, 471–474, doi:10.1029/GL014i004p00471.

Bahnsen, A., M. Jespersen, E. Ungstrup, B. M. Pedersen, and L. Eliasson (1989), Viking observations at the source region of auroral kilometric radiation, *J. Geophys. Res.*, *94*, 6643–6654, doi:10.1029/JA094iA06p06643.

Benson, R. F., and W. Calvert (1979), Isis 1 observations at the source of auroral kilometric radiation, *Geophys. Res. Lett.*, *6*, 479–482.

Calvert, W. (1981), The AKR emission cone at low frequencies, *Geophys. Res. Lett.*, *8*, 1159–1162.

Calvert, W. (1987), Hollowness of the observed auroral kilometric radiation pattern, *J. Geophys. Res.*, *92*, 1267–1270.

de Feraudy, H., and R. Schreiber (1995), Auroral radiation ray distribution in the light of Viking observations of AKR, *Geophys. Res. Lett.*, *22*, 2973–2976.

de Feraudy, H., B. M. Pedersen, A. Bahnsen, and M. Jespersen (1987), Viking observations of auroral kilometric radiation from the plasmasphere to night auroral oval source regions, *Geophys. Res. Lett.*, *14*, 511–514.

Delory, G. T., R. E. Ergun, C. W. Carlson, L. Muschietti, C. C. Chaston, W. Peria, J. P. McFadden, and R. Strangeway (1998), FAST observations of electron distributions within AKR source regions, *Geophys. Res. Lett.*, *25*, 2069–2072, doi:10.1029/98GL00705.

Denton, R. E., J. D. Menietti, J. Goldstein, S. L. Young, and R. R. Anderson (2004), Electron density in the magnetosphere, *J. Geophys. Res.*, *109*, A09215, doi:10.1029/2003JA010245.

Ergun, R. E., et al. (1998), FAST satellite wave observations in the AKR source region, *Geophys. Res. Lett.*, *25*, 2061–2064, doi:10.1029/98GL00570.

Green, J. L., and D. L. Gallagher (1985), The detailed intensity distribution of the AKR emission cone, *J. Geophys. Res.*, *90*, 9641–9649.

Green, J. L., D. A. Gurnett, and S. D. Shawhan (1977), The angular distribution of auroral kilometric radiation, *J. Geophys. Res.*, *82*, 1825–1838.

Gurnett, D. A. (1974), The Earth as a radio source: Terrestrial kilometric radiation, *J. Geophys. Res.*, *79*, 4227–4238.

Gurnett, D. A., et al. (2001), First results from the Cluster wideband plasma wave investigation, *Ann. Geophys.*, *19*, 1259–1272.

Hanasz, J., H. de Feraudy, R. Schreiber, G. Parks, M. Brittnacher, M. M. Mogilevsky, and T. V. Romantsova (2001), Wideband bursts of auroral kilometric radiation and their association with UV auroral bulges, *J. Geophys. Res.*, *106*, 3859–3872, doi:10.1029/2000JA900098.

Haselgrove, J. (1963), The Hamiltonian ray path equations, *J. Atmos. Terr. Phys.*, *25*, 397–399, doi:10.1016/0021-9169(63)90173-9.

Huff, R. L., W. Calvert, J. D. Craven, L. A. Frank, and D. A. Gurnett (1988), Mapping of auroral kilometric radiation sources to the aurora, *J. Geophys. Res.*, *93*, 11,445–11,454.

Louarn, P., and D. Le Quéau (1996), Generation of the auroral kilometric radiation in plasma cavities—I. Experimental study, *Planet. Space Sci.*, *44*, 199–210.

Mutel, R. L., W. M. Peterson, T. R. Jaeger, and J. D. Scudder (2007), Dependence of CMI growth rates on electron velocity distributions and perturbation by solitary waves, *J. Geophys. Res.*, *112*, A07211, doi:10.1029/2007JA012442.

Mutel, R. L., I. W. Christopher, and J. S. Pickett (2008), Cluster multispacecraft determination of AKR angular beaming, *Geophys. Res. Lett.*, *35*, L07104, doi:10.1029/2008GL033377.

Pedersen, B. M., R. Pottelette, L. Eliasson, J. S. Murphree, R. D. Elphinstone, A. Bahnsen, and M. Jespersen (1992), Auroral kilometric radiation from transpolar arcs, *J. Geophys. Res.*, *97*, 10,567–10,573, doi:10.1029/92JA00410.

Pritchett, P. L., R. J. Strangeway, R. E. Ergun, and C. W. Carlson (2002), Generation and propagation of cyclotron maser emissions in the finite auroral kilometric radiation source cavity, *J. Geophys. Res.*, *107*(A12), 1437, doi:10.1029/2002JA009403.

Schreiber, R. (2005), A simple model of the auroral kilometric radiation visibility, *J. Geophys. Res.*, *110*, A11222, doi:10.1029/2004JA010903.

Schreiber, R., O. Santolik, M. Parrot, F. Lefeuvre, J. Hanasz, M. Brittnacher, and G. Parks (2002), Auroral kilometric radiation source characteristics using ray tracing techniques, *J. Geophys. Res.*, *107*(A11), 1381, doi:10.1029/2001JA009061.

Treumann, R. A. (2006), The electron cyclotron maser for astrophysical application, *Astron. Astrophys. Rev.*, *13*, 229–315, doi:10.1007/s00159-006-0001-y.

Tsyganenko, N. A. (1989), A magnetospheric magnetic field model with a warped tail current sheet, *Planet. Space Sci.*, *37*, 5–20.

I. W. Christopher, K. A. Hutchinson, J. D. Menietti, and R. L. Mutel, Department of Physics and Astronomy, University of Iowa, Iowa City, IA 52242, USA. (iver-christopher@uiowa.edu; kent-hutchinson@uiowa.edu; john-menietti@uiowa.edu; robert-mutel@uiowa.edu)